JACS
JOURNAL OF THE AMERICAN CHEMICAL SOCIETY

pubs.acs.org/JACS

Article

Isolation and Crystallographic Characterization of an Octavalent Co_2O_2 Diamond Core

Joseph E. Schneider, Shilin Zeng, Sophie W. Anferov, Alexander S. Filatov, and John S. Anderson*

Cite This: J. Am. Chem. Soc. 2024, 146, 23998−24008

Read Online

ACCESS | Metrics & More | Article Recommendations | Supporting Information

ABSTRACT: High-valent cobalt oxides play a pivotal role in alternative energy technology as catalysts for water splitting and as cathodes in lithium-ion batteries. Despite this importance, the properties governing the stability of high-valent cobalt oxides and specifically possible oxygen evolution pathways are not clear. One root of this limited understanding is the scarcity of high-valent Co(IV)-containing model complexes; there are no reports of stable, well-defined complexes with multiple Co(IV) centers. Here, an oxidatively robust fluorinated ligand scaffold enables the isolation and crystallographic characterization of a $Co(IV)_2$-bis-μ-oxo complex. This complex is remarkably stable, in stark contrast with previously reported $Co(IV)_2$ species that are highly reactive, which demonstrates that oxy-$Co(IV)_2$ species are not necessarily unstable with respect to oxygen evolution. This example underscores a new design strategy for highly oxidizing transition-metal fragments and provides detailed data on a previously inaccessible chemical unit of relevance to O−O bond formation and oxygen evolution.

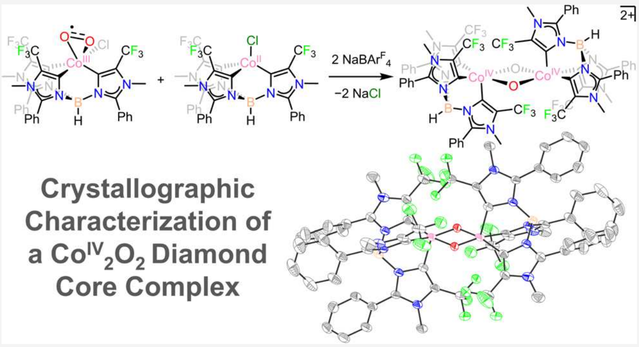

INTRODUCTION

High-valent cobalt complexes have been a topic of intense interest recently due to their relevance to oxygen evolution reactivity. This reaction is a critical step in the generation of sustainable fuels and energy sources,[1−4] and it is also a decay pathway limiting the voltage of metal-oxide cathodes.[5] Cobalt-oxide films have emerged as notable platforms for the electrochemical oxidation of water to form gaseous oxygen,[6−8] and the key intermediates that are typically invoked in these systems are high-valent, formally Co(IV) or higher, Co-oxo complexes.[4,9−15] Despite the importance of highly oxidized Co complexes,[16−19] Co(IV) complexes of relevance to O_2 activation or evolution (oxos, superoxos, peroxos, etc.) are rare.

Oxygenation of Co complexes does not typically generate species with oxidation states greater than III. Specifically, Co(II) complexes commonly activate O_2 to form either Co(III)-superoxide complexes or bridging $Co(III)_2$-peroxide complexes.[20,21] Co(III)-superoxide complexes can further react via H atom abstraction to form Co(III)-hydroperoxide complexes,[22−24] but there is only one report of an oxygenated Co(III)-superoxide complex being further converted into a Co(IV) complex.[25] Protonation and/or reduction of $Co(III)_2$-peroxide complexes can lead to cleavage of the O−O bond; Co(IV) intermediates are invoked in these reactions but only terminal Co(III) products have been observed.[15,26] This contrasts with similar $Fe(III)_2$-peroxide complexes, which can cleave the O−O bond and form dimers with octavalent $Fe(IV)_2$ cores.[27−29] Bridging $Co(III)_2$-peroxide complexes can be oxidized to superoxide complexes, and further oxidation typically results in the loss of dioxygen, not the isolation of Co(IV) species.[20,30−33]

Co(IV) complexes with oxygen-based ligands have most commonly been generated via oxidative pathways. Co oxide cuboidal clusters can be oxidized to form stable complexes with a single Co(IV) center and an average oxidation state of Co(3.25).[34,35] Doubly oxidized, $Co(IV)_2Co(III)_2$ cuboidal clusters have been spectroscopically characterized under oxidative electrochemical polarization, but this potential must be maintained in order to observe the oxidized species.[36,37] Other attempts to identify $Co(IV)_2$ species were noted to result in the evolution of oxygen gas.[38] Nam and co-workers demonstrated the formation of a Co(IV)-oxo complex via the oxidation of a Co(II)-aquo species.[39] While this represents a rare oxy-Co(IV) complex, the instability of this compound has limited characterization to in situ spectroscopic methods that has made firm assignment of its structure challenging.[40] Similarly, previous results from this laboratory generated a

Received: May 29, 2024
Revised: August 1, 2024
Accepted: August 2, 2024
Published: August 15, 2024

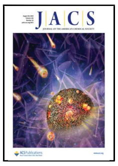

ACS Publications

https://doi.org/10.1021/jacs.4c07335

Scheme 1. Synthesis of Complexes 1 and 2

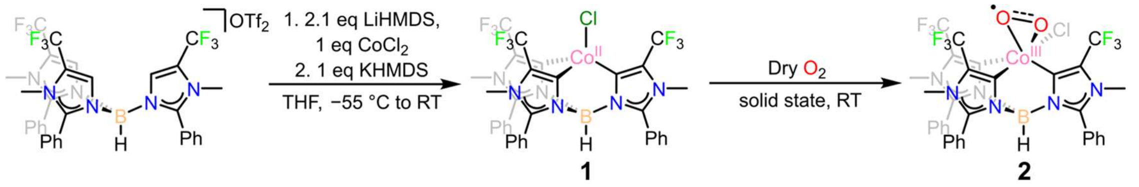

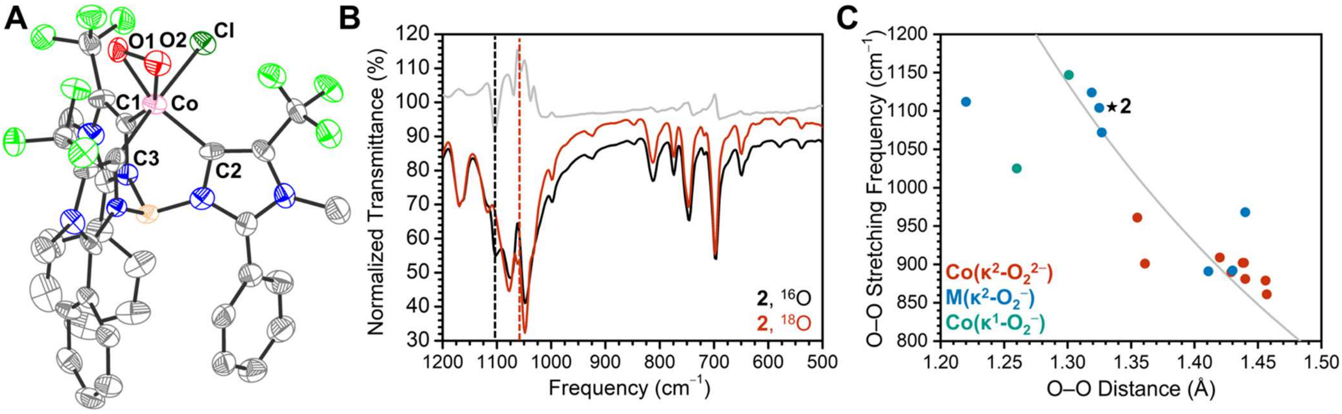

Figure 1. (A) Crystal structure of **2**. Hydrogen atoms bound to carbon atoms and cocrystallized solvent removed for clarity. Selected bonds (in Å): O1−O2 = 1.335(12), Co−O1 = 1.955(8), Co−O2 = 1.917(8), Co−Cl = 2.285(3); Co−C1 = 1.936(10); Co−C2 = 1.955(10), Co−C3 1.961(10). (B) IR spectra of ^{16}O-2 (black) and ^{18}O-2 (red) of **2** with the shift of the O−O stretching frequency at 1102 cm^{-1} shown. (C) Plot of the O−O stretching frequency against the O−O bond length for **2** (black star), end-on Co(III)-superoxides (teal), side-on Co(III)-peroxides (red), and side-on metal−dioxygen complexes more generally (green). Data from refs 22,51−62,66,67 The gray curve gives a fit to Badger's rule, $L = 75.78\nu^{-2/3} + 0.60$. Note that the fit includes O_2, which is not shown, as it is not within the plotted values.

Co(IV)-oxo complex from a Co(II)-hydroxide complex, but this compound decays rapidly even at cryogenic temperatures.[41] Recently, Wang and co-workers made a key step forward with the report of a mixed-valent Co(IV)−Co(III) dimer.[42,43] This complex can be generated and studied at low temperatures; however, thermal instability similarly prevents the isolation or crystallographic characterization of this species. Thus, no isolated or crystallographically characterized cobalt-oxo complex has been reported containing all-Co(IV) centers.

One key challenge in this area is intramolecular ligand C−H bond oxidation, and this has been noted as a general problem in the isolation and study of highly oxidizing species.[44] A key example comes from Theopold and co-workers who showed that while a Co(I) scorpionate complex can dimerize with O_2 to form a $Co(III)_2$-bis-μ-oxo core, isolation of this dimer is not possible due to oxidation of a flanking isopropyl group.[45] This decay pathway has also been observed for a Co(IV)-imide complex and the Co(IV)-oxo complex from our laboratory mentioned above,[16,41] among many related examples in the literature.

To meet this challenge, we recently developed a new oxidatively stable scorpionate ligand scaffold, tris(4-trifluoromethyl-3-methyl-2-phenylimidazol-5-ylidene)borate ($[(HB(^{CF_3,Ph}mIm)_3)]^-$, Scheme 1).[46] This scaffold uses oxidatively robust fluoroalkyl flanking groups on mesoionic carbene arms and has strong donor properties suitable for the isolation of high-valent transition-metal complexes. We were interested in understanding how this scaffold might support various oxygenated intermediates, particularly those of possible relevance to O_2 evolution, in addition to understanding how this system could stabilize high oxidation-state species more generally. Here, we find that a Co(II)-chloride complex of this ligand forms a stable Co(III)-superoxide adduct with dioxygen. Further activation of this dioxygen unit with a second equivalent of Co(II)-chloride breaks the O−O bond to generate a highly oxidized octavalent $Co(IV)_2$-bis-μ-oxo dimer. Despite the thermodynamic potency of this core as a H atom abstractor, this complex displays remarkable stability, which demonstrates how fluorinated ligand scaffolds can be used to stabilize highly oxidized materials. Furthermore, the isolation of this complex demonstrates that $Co(IV)_2$-oxo complexes are not necessarily unstable with respect to O−O coupling.

■ RESULTS AND DISCUSSION

Metalation and Synthesis of a Co(III) Superoxide Complex. We synthesized Co(II)-chloride complex **1** with a two-step metalation procedure (Scheme 1). Deprotonation of the proligand $[HB(^{CF_3,Ph}mIm)_3H_3](OTf)_2$ with two equivalents of lithium hexamethyldisilazide followed by addition of $CoCl_2$ and stirring overnight yields a blue precipitate. This material has not been thoroughly characterized, but we identify it as a complex with two ligand arms coordinated to Co and one unligated and protonated arm, $[Co^{II}(\kappa^2\text{-}HB\text{-}(^{CF_3},PhmIm)_3H)Cl_2]$, based on nuclear magnetic resonance (NMR) spectroscopy and single-crystal X-ray diffraction (SXRD) structure determination. This intermediate blue precipitate is observed even if three equivalents of LiHMDS are used for deprotonation. Stirring a slurry of this intermediate in THF with one equivalent of potassium hexamethyldisilazide for 4 h yields the Co(II)-chloride complex $[Co^{II}(HB(^{CF_3,Ph}mIm)_3)Cl]$ (**1**) based on NMR, infrared (IR), and electron paramagnetic resonance (EPR) spectroscopy; SXRD structure determination; and elemental analysis (see Experimental Section and Supporting Information).

Complex **1** slowly turns from blue to brown upon exposure to dry O_2 in the solid state (Scheme 1). The product of this reaction was identified as the side-on Co(III)-superoxide complex $[Co^{III}(HB(^{CF_3,Ph}mIm)_3)Cl(\eta^2\text{-}O_2^{\bullet})]$ (**2**) by a suite of techniques discussed below. Superoxide complexes have been identified as intermediates in both O_2 evolution and reduction reactions.[12,15,47−50] Thus, the properties of **2** and the degree of O_2 activation in this species are metrics of interest.

Diffusion of pentane into a saturated solution of **2** in DCM at −35 °C yields crystals suitable for structural determination by X-ray diffraction (Figure 1A). The structure supports the assignment of a side-on complex with an O···Å bond length of 1.335(12) Å. The side-on binding of **2** is unusual for a Co(III)-superoxide adduct; previously reported Co(III)-superoxide complexes invariably display end-on binding.[21,51−54] Conversely, there are several reports of side-on Co(III)-peroxides.[55−63] This may partly be a result of the coordination number. Co(III)-superoxide adducts have typically been supported with macrocyclic ligands that disfavor two adjacent binding sites necessary for side-on dioxygen binding. Nonetheless, the absence of side-bound superoxide complexes represents an interesting gap in Co-O_2 coordination chemistry. The observed O−O bond length in **2** is long for a superoxide moiety, meriting the evaluation of a possible Co(IV)-peroxide character.

IR spectra with both $^{16}O_2$ and $^{18}O_2$ isotopologues reveal an isotope-dependent peak that occurs at 1103 cm^{-1} for the lighter isotopologue and ~40 cm^{-1} lower in frequency for the heavier congener (Figure 1B). This frequency region and shift are consistent with the assignment of a superoxide ligand.[21] We also observe a peak at 416 cm^{-1} that is ~5 cm^{-1} lower in energy with $^{18}O_2$ labeled material; this is assigned to a Co−(O_2) stretch (see Figure S16). We note that these observed isotopic shifts are smaller than those predicted by ideal harmonic oscillators (60 and 15 cm^{-1}, respectively). We attribute these diminished shifts to mixing with C−F stretching modes, and this conclusion is supported by density functional theory (DFT) analysis (see Figure S17).

X-band EPR spectroscopy further supports a superoxide assignment. The room-temperature spectrum of **2** reveals an isotropic signal with $g = 2.03$ and an 8-line pattern consistent with hyperfine coupling of 32 MHz to a single ^{59}Co nucleus (see Figure S25). This spectrum supports the assignment of an $S = 1/2$ Co complex with a ligand-centered radical. The magnitude of the hyperfine coupling is similar to previously reported end-on superoxide complexes, which typically have isotropic ^{59}Co hyperfine coupling of <45 MHz.[21] Moreover, comparison of ^{59}Co hyperfine couplings with **1** as a control with all spin centered on Co suggests that <30% of the spin in **2** is located on Co (see Figures S24 and S25), supporting the assignment of a superoxide adduct.[53,64,65]

Figure 1C and Table 1 compare the O−O vibrational energy and bond length of **2** with other known transition-metal−dioxygen adducts,[22,51−62,66,67] alongside a Badger's rule fit to these data that is similar to previous literature analyses.[68,69] Complex **2** has an O−O vibrational frequency much greater than that typical for peroxide complexes but well within the range of that for a superoxide complex. The length of the O−O bond, while longer than those measured for end-on cobalt-superoxide complexes, is still typical for superoxide complexes more generally. Overall, all analyses—SXRD, IR spectroscopy, and EPR spectroscopy—support the assignment of **2** as a side-on Co(III)-superoxide complex. DFT also predicts that the majority of the spin density is located on the superoxide ligand (Figure S40).

Table 1. Comparison of Selected Co(III)-Superoxide and Co(III)-Peroxide Complexes[a]

	ν_{O-O}	L_{O-O}	refs
2	1105	1.335(12)	this work
$[Co^{III}(Tp^{iPr,Me})(\eta^2\text{-}O_2)]$	961	1.355(3)	55,71
$[Co^{III}(tmen)_2(\eta^2\text{-}O_2)]^+$	861[b]	1.457(3)	62
$[Co_2{}^{III}(CN)_4(Pme_2Ph)_5(\eta^2\text{-}O_2)]$	881[b]	1.44	60
$[Co^{III}(TBDAP)(\eta^2\text{-}O_2)]^+$	879	1.456(3)	57
$[Co^{III}(TIMEN^{xyl})Co(\eta^2\text{-}O_2)]^+$	890	1.429(3)	56
$[Co^{III}(2{=}phos)_2(\eta^2\text{-}O_2)]^+$	909[b]	1.42(1)	59
$[Co^{III}(NacNAc^{Dipp,tBu})(\eta^2\text{-}O_2)]$	901	1.361(5)	58
$[Co^{III}(12\text{-}TMC)(\eta^2\text{-}O_2)]^+$	902	1.439(2)	61
$[Co^{III}(13\text{-}TMC)(\eta^2\text{-}O_2)]^+$	902	1.438(4)	61
$[Co^{III}(TPA)(\eta^2\text{-}O_2)]^{+A}$	845	[d]	63
$[Co^{III}(Tp^{me2})(L^{Ph})(\eta^1\text{-}O_2^{\bullet})]$	1147	1.301(5)	51
$[Co^{III}(acacen)(py)(\eta^1\text{-}O_2^{\bullet})]$	1025	1.26(4)[c]	52,54,66

[a] Headers are, respectively, the O−O stretching frequency ν_{O-O} (cm^{-1}), the O−O bond length L_{O-O} (Å), and references. [b] Not confirmed by isotopic labeling. [c] Determined with bzacen in place of acacen. [d] No experimental bond length reported.

While Co(III)-superoxide complexes typically release O_2 readily,[21] we observe that **2** is stable to vacuum. Co(II) oxidation potentials and O_2 binding affinities are often correlated, which provides a way to assay the origin of this irreversible O_2 binding in **2**.[70] The cyclic voltammogram of **1** exhibits a quasi-reversible reduction with a peak oxidative current at −0.7 V vs Fc/Fc$^+$ (see Figure S28). Because this potential is within the range of other Co(II) complexes that reversibly bind dioxygen (reversible $E_{1/2}$ of approximately −0.6 to −1.0 V vs Fc/Fc$^+$), the stability of **2** does not arise from a more favorable reduction of O_2 to a superoxide anion.[70] It is therefore likely that the additional stability of **2** is due to the unusual side-on binding mode, which provides an additional contact between the superoxide ligand and the metal center. This is consistent with the superoxide ligand **2** being similarly activated to other Co(III)-superoxide complexes, as suggested by the typical values **2** displays for the O−O stretching frequency and the ^{59}Co hyperfine coupling.[22,51−62,66,67]

Formation of an Octavalent Co_2O_2 Diamond Core. Oxygenated Co complexes are known to spontaneously dimerize in solution and thereby further activate the O_2 unit.[20,21] Theopold and co-workers observed such a dimerization with a scorpionate ligand whose isopropyl groups resemble the steric profiles of trifluoromethyl groups.[45,72,73] However, the resulting Co(III)$_2$-bis-μ-oxo complex decays through the oxidation of a C−H bond on the flanking isopropyl groups. In contrast, unlike many Co(III)-superoxide complexes, complex **2** is stable in solution at room temperature. We ascribe this stability to the irreversible binding of dioxygen, which prevents spontaneous dimerization.

We rationalized that dimerization and further activation of the dioxygen moiety might occur upon the addition of nonoxygenated complex **1**, particularly in the presence of a halide abstractor. Indeed, slow addition of **1** cosolubilized in DCM with 2 equiv of sodium tetrakis(3,5-bistrifluoromethylphenyl)borate ($[BAr_4^F]^-$) to a chilled solution of **2** in DCM results in a deep green solution. ^1H and $^{19}F\{^1H\}$ NMR spectroscopies suggest that this mixture produces one major paramagnetic product, **3**, and analysis by

Scheme 2. Dimerizations of 1 and 2 to Generate Bis-μ-oxo Complex 3 and Subsequent Reduction to Bis-μ-hydroxo Complex 4

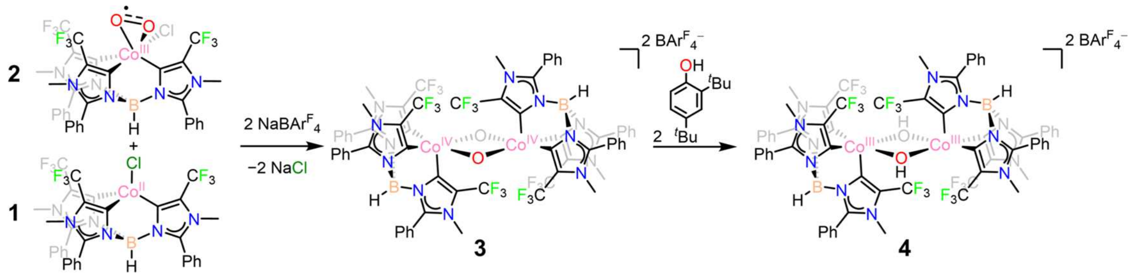

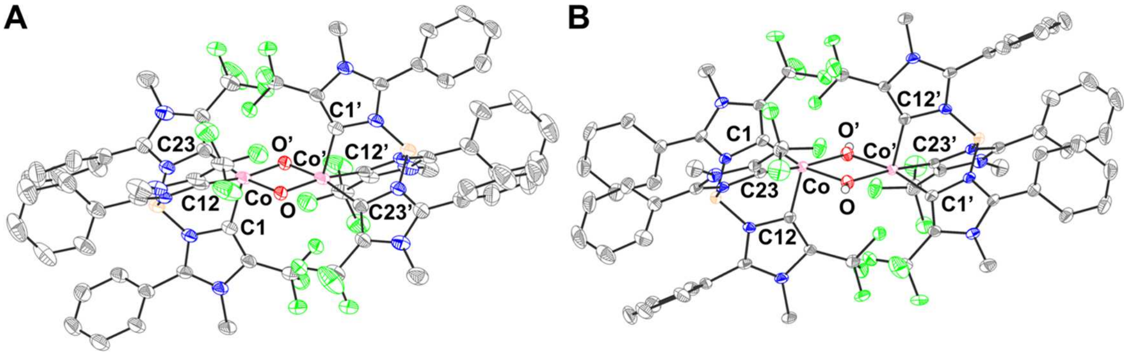

Figure 2. Structures of diamond core complexes 3 and 4. Hydrogens bound to carbon, cocrystallized solvent, and $[BAr_4^F]^-$ counteranions are omitted for clarity. (A) 3 Co1−Co1′ = 2.6801(8) Å, Co1−O1 = 1.832(2) Å, Co1−O1′ = 1.836(2) Å, Co1−C1 = 1.926(3) Å; Co1−C12 = 1.976(3) Å; Co1−C23 = 1.974(3) Å. The Co centers are equivalent by inversion symmetry, and C1 is located on the axial carbene. (B) 4 Co1−Co1 = 2.980(1) Å, Co1−O1 = 1.885(3) Å, Co1−O1 = 1.892(3) Å, Co1−C1 = 1.920(4) Å; Co1−C12 = 1.888(4) Å; Co1−C23 = 1.948(4) Å. The Co centers are equivalent by inversion symmetry and C12 is located on the axial carbene.

the Evans method shows a μ_{eff} of 2.8 Bohr magnetons (calculated for a dimeric product). This magnetic susceptibility matches the expected spin-only value for a triplet (see Figure S6).[74−76] This product is indefinitely stable in DCM solution at −78 °C, although it bleaches slowly at room temperature in solution. No reactivity is observed between **3** and weak C−H bonds, such as 9,10-dihydroanthracene or 1,4-cyclohexadiene. However, the addition of 2,4-di-*tert*-butylphenol to a solution of **3** causes the solution to bleach to a lighter shade of green (see Figure S30). ^1H and $^{19}F\{^1H\}$ NMR spectroscopies reveal the formation of a single diamagnetic product, **4**. Based on these NMR spectra, as well as additional spectroscopic and structural evidence discussed below, **3** is assigned as a Co(IV)$_2$-bis-μ-oxo complex and **4** as a Co(III)$_2$-bis-μ-hydroxo complex (Scheme 2).

Fortunately, we were able to grow crystals suitable for SXRD analysis of both **3** and **4** (Figure 2). Both complexes have a diamond core structure, with two square-pyramidal Co centers that are equivalent by a molecular inversion center (τ_5 = 0.02 for **3** and 0.03 for **4**). The presence of one $[BAr_4^F]^-$ counteranion per Co indicates that both dimers are dicationic. DOSY NMR analysis on diamagnetic **4** reveals a slower diffusion constant than a reference monomeric complex that suggests **4** remains a dimer in solution (see Figures S12 and S13).

Geometric changes support our assignment that the Co_2O_2 core in **3** is more highly oxidized than that in **4** (see Table S6). The Co−Co distance in **3** is 2.6801(9) Å; this is much shorter than the Co−Co distance of 2.9804(9) Å in **4**. Complex **3** also has somewhat shorter Co−O lengths (1.833(2) and 1.836(2) Å) than the corresponding bond distances in **4** (1.885(2) and 1.892(2) Å). The Co−Co distance in **4** is longer than might be expected from previously reported Co(III)$_2$ hydroxide dimers due to the absence of a carboxylate bridge in **4**.[77,78] Furthermore, the O−H hydrogen atoms in **4** are visible in the difference Fourier map and can be freely refined without using any restraints. There is no obvious analogous residual electron density in the structure of **3**. IR spectroscopy also supports the absence of the O−H bonds in **3** (see Figure S22). IR spectroscopy on both ^{16}O and ^{18}O isotopologues reveals potential differences in the regions where DFT predicts Co_2O_2 stretches, but convolutions with other ligand-based stretches make concrete assignments difficult (see Figure S19).

This assignment of **3** as a Co(IV)$_2$-bis-μ-oxo complex is supported by X-ray absorption spectroscopy (XAS). There is an ∼1 eV shift in the edge energy upon dimerization to form **3** (Figure 3A, see also Figure S31). These edge shifts support the idea that **3** contains Co centers that are oxidized beyond the Co(III) oxidation state found in **2**. The more intense 1s to 3d XANES pre-edge signal in **3** is indicative of a change to a square-pyramidal geometry, with consequently greater 3d-4p mixing.[79] TD-DFT calculations support this increased intensity, and these calculations also reproduce the relative energy of each compounds' maximum XANES absorption (see Figure S32).

The extended X-ray absorption fine structure (EXAFS) spectrum of **3** further corroborates the formation of a diamond core complex with a short Co−Co distance (Figure 3B). This data can be fit with five first-sphere Co−C/O scatterers at an average distance of 1.90 Å, three second-sphere Co−N scatterers at an average distance of 2.82 Å, and one Co−Co scatterer at 2.56 Å. The difference between this EXAFS measurement of the Co−Co distance and the 2.6801(9) Å distance observed crystallographically may arise from several reasons, such as the solid-state packing in the crystal. Nevertheless, both measurements support that the Co−Co

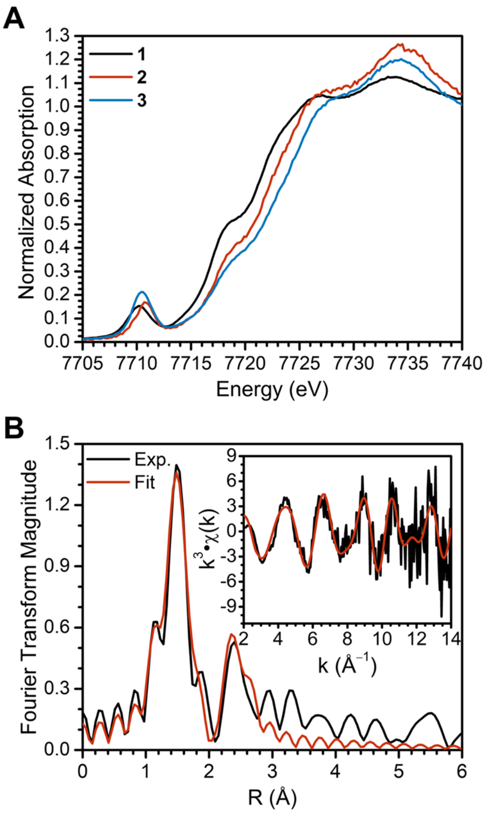

Figure 3. (A) Co K-edge spectra of peaks 1, 2, and 3. (B) Fourier transform EXAFS spectrum and fit of **3** along with the spectrum and fit in *k*-space (inset). The fit indicates a Co−Co bond distance of 2.6 Å.

distance in **3** is substantially shorter than the Co−Co distance in **4** as well as the ~2.8 Å Co−Co distance estimated for the single literature example of a Co(III)−Co(IV)-bis-μ-oxo complex.[42]

Altogether, these spectroscopic and crystallographic data strongly support the assignment of **3** as a $Co(IV)_2$-bis-μ-oxo complex. Both SXRD and XAS methods suggest a Co−Co distance shorter than 2.7 Å, which is substantially shorter than the Co−Co distance of $Co(III)_2$ complex **4** as well as literature reports of the Co−Co distance for a Co(III)−Co(IV) diamond core complex.[42] The NMR spectra of **3** are clearly paramagnetic, and the Evans method is supportive of a high-spin triplet ground state. Such a triplet state in **3** is inconsistent with diamagnetic Co(III) centers (as observed in **4**). The presence of Co centers with an oxidation state higher than III is further corroborated by the Co K-edge energy. Complex **3** is also silent by X-band EPR spectroscopy that is inconsistent with a possible mixed-valent Co(III)−Co(IV) assignment (see Figure S26). Thus, the most plausible assignment for **3** is a $Co(IV)_2$-bis-μ-oxo complex.

DFT analysis of **3** supports the experimental data presented. Calculations predict a triplet ground state, which is consistent with our assignment. Interestingly, the unpaired spin density in **3** is not localized to a matching pair of orbitals on each cobalt center. One unpaired electron resides in a Co−Co/Co−O σ^* orbital, while the other resides in a Co−O π^* orbital, and each of these orbitals has O-character (see Figure S41). The resulting spin distribution is evenly divided around the Co_2O_2 core (see Figure S42). This raises the possibility of a Co(III)−Co(IV) complex with a delocalized μ-oxo-μ-oxyl bridging ligand as a plausible assignment, but additional experiments and analyses are required to concretely explore this possibility.

The apparent stability of **3** is notable in comparison to prior literature reports. For instance, the $Co(III)_2$-bis-μ-oxo complexes formed from the analogous activation of oxygen by Co(I) tris(pyrazolyl)borate complexes decay via oxidation of ligand C−H bonds.[45] A similar decay pathway is observed in a monomeric Co(IV)-oxo complex supported by a similarly strongly donating triscarbeneborate ligand.[41] We propose this stability toward intramolecular ligand oxidation arises from the trifluoromethyl flanking groups that are oxidatively robust. Indeed, these flanking groups may in fact result in over-stabilization as **3** does not react with 9,10-dihydroanthracene or 1,4-cyclohexadiene to form **4**. The formation of **4** from the reaction with 2,4-di-*tert*-butylphenol suggests that this is a kinetic limitation in the reactivity of **3**, not a thermodynamic one. The O−H bond in 2,4-di-*tert*-butylphenol is stronger (BDE 86 kcal/mol) than the C−H bonds we tested (BDEs ~ 80 kcal/mol), but O−H bonds are kinetically more reactive for many systems.[80−82] Thus, **3** is a thermodynamically potent H atom abstractor but only reacts with a kinetically favorable substrate. DFT supports this hypothesis; despite the absence of C−H oxidation reactivity, **3** is expected to be a thermodynamically potent H atom abstractor as each O−H bond strength in **4** is calculated at ~100 kcal/mol (as referenced to phenol, see Table S7).[80] Therefore, regardless of the mechanism of 2,4-di-tert-butylphenol oxidation, the absence of reactivity between **3** and C−H bonds is not attributable to an insufficient thermodynamic driving force. We hypothesize this kinetic stability of **3** toward intermolecular C−H oxidation is due to steric protection of the oxo ligands. A percent buried volume calculation indeed shows that the oxygen atoms are 92% buried (see Figure S44).[83] Thus, the oxidative robustness and steric profile of the trifluoromethyl groups appear to shield the oxo bridges from the solvent and other reagents.

When Co oxide cuboidal clusters are oxidized to the point of containing two Co(IV) centers, they are known to decay back to an all-Co(III) state, likely through the formation of O−O bonds and release of hydrogen peroxide or dioxygen.[36,38] Similarly, overcharging $LiCoO_2$ cathodes can lead to loss of oxygen.[5] Our ability to form **3** from the activation of dioxygen clearly indicates that this is not a thermodynamically favorable decay pathway. The reasons for this stability are not entirely clear, but it may simply be due to the strong donor properties of the supporting scorpionate ligand, stabilizing the $Co(IV)_2O_2$ unit. Alternatively, we hypothesize the stability may be due to the lack of terminal oxo ligands that are typically invoked in the formation of O−O bonds in water oxidation.[12,36,38] This hypothesis motivates additional studies of high-valent Co complexes to better understand the factors governing O−O bond coupling.

CONCLUSIONS

We report the isolation of an octavalent Co(IV) moiety, along with its crystallographic characterization. This complex is formed through the stepwise activation of dioxygen by a Co(II)-chloride complex, first to form a Co(III)-superoxide complex followed by further reduction of the dioxygen unit and O−O bond cleavage by dimerization with another equivalent of Co(II)-chloride. The resulting $Co(IV)_2$-bis-μ-oxo complex can be reduced to form the analogous $Co(III)_2$-bis-μ-hydroxo complex with suitable H atom donors. These assignments are supported by crystallographic characterization as well as NMR, EPR, and X-ray absorption spectroscopies. The isolation of the $Co(IV)_2$-bis-μ-oxo complex is enabled through the use of a highly donating scorpionate ligand featuring flanking perfluoroalkyl groups. These oxidatively robust flanking groups encapsulate and protect the reactive octavalent diamond core. The inherent stability of this complex to loss of dioxygen is intriguing and motivates further studies of the factors governing the stability of dicobalt(IV) cores and the formation of O−O bonds.

■ EXPERIMENTAL SECTION

All manipulations were performed under a dry nitrogen atmosphere using either standard Schlenk techniques or an mBraun Unilab Pro glovebox unless otherwise stated. All chemicals were obtained from commercial sources and used as received, unless otherwise stated. The proligand $[HB(^{CF_3,Ph}mImH)_3](OTf)_2$ was synthesized according to a previously reported procedure.[46] Sodium tetrakis[3,5-bis-(trifluoromethyl)phenyl]borate ($Na[BAr_4^F]$) was dried under vacuum at 100 °C prior to use. All solvents except for 1,2-difluorobenzene were dried on a solvent purification system from Pure Process Technologies before being stored over 4 Å molecular sieves under N_2. Tetrahydrofuran (THF) and diethyl ether (Et_2O) were stirred over NaK alloy and passed through a plug of activated alumina prior to storing over 4 Å sieves under N_2. 1,2-Difluorobenzene was purified with acidified potassium permanganate (CAUTION: exothermic reaction), washed with water, dried with anhydrous magnesium sulfate, distilled from calcium hydride, and stored over 4 Å molecular sieves under N_2.

^1H, $^{11}B\{^1H\}$, $^{13}C\{^1H\}$, and $^{19}F\{^1H\}$ NMR spectra were collected on a 400 MHz Bruker DRX spectrometer equipped with a BBO probe, with the exception of the $^{13}C\{^1H\}$ spectrum of **4** that was collected on a 500 MHz Bruker Avance-III-HD spectrometer equipped with a BBFO SmartProbe. ^1H and $^{13}C\{^1H\}$ spectra were referenced to the appropriate solvent peaks. DOSY spectra were collected with a pulse sequence that utilized a double stimulated echo for convection compensation. CW-EPR spectra were collected on a Bruker Elexsys 500 3500 spectrometer with an X-band dual mode resonator and simulated using EPRsim.[84] IR spectra were collected as solids on a Bruker α II instrument using a Platinum Diamond ATR module. Ultraviolet−visible (UV−vis) spectra were recorded on a Thermo Scientific Evolution 300 spectrometer. Electrochemical measurements were made using a BAS Epsilon potentiostat with a glassy carbon working electrode, platinum wire counter electrode, and silver wire pseudoreference electrode. Combustion analysis was performed by Midwest Microlabs with sample manipulation occurring in a glovebox with at most 40 ppm oxygen. High-resolution mass spectroscopy was performed with an Agilent 6224 TOF instrument with electrospray ionization.

Synthetic Procedures. *Synthesis of 1.* A suspension of $[HB(^{CF_3,Ph}mImH)_3](OTf)_2$ (0.75 g, 0.76 mmol) in 15 mL of tetrahydrofuran was chilled to −55 °C. Lithium hexamethyldisilazide (0.27 g, 1.6 mmol) was added as a solid, and the reaction was stirred cold until homogeneous, for approximately 15 min. Anhydrous $CoCl_2$ (0.10 g, 0.76 mmol) was added as a solid, and the reaction mixture was stirred at room temperature overnight. The resulting blue powder was filtered out from the solution, washed with THF, and dried under vacuum (520 mg, 0.64 mmol, 86% yield). ^1H NMR (CD_2Cl_2, 400 MHz): δ 12.1 (6H, Me-*H*), δ 9.9 (2H, Ph-*H*), δ 9.4 (2H, Ph-*H*), δ 9.3 (2H, Ph-*H*), 7.7 (2H, Ph-*H*), 7.5 (1H, Imid-*H* of Ph-*H*), 7.4 (1H, Imid-*H* or Ph-*H*), 7.2 (2H, Ph-*H*), 6.7 (2H, Ph-*H*), 3.1 (3H, Me-*H*). $^{19}F\{^1H\}$ NMR (CD_2Cl_2, 400 MHz): δ 31.7 (6F), −52.9 (3F). We do not observe a signal from the B-*H* proton by ^1H NMR spectroscopy. One pair of Ph-*H* peaks is also not observed by ^1H NMR spectroscopy; we believe this peak is plausibly too broad to conclusively identify underneath the other Ph-*H* peaks. Crystals suitable for SXRD were grown by vapor diffusion of pentane into saturated dichloromethane. Without any further characterization or purification, this blue powder was suspended in 15 mL of tetrahydrofuran, and potassium hexamethyldisilazide (0.13 g, 0.64 mmol) was added as a solid. The mixture was stirred at room temperature for 4 h. The resulting blue powder was filtered onto Celite, washed with tetrahydrofuran, and extracted with acetonitrile. The green acetonitrile solution was concentrated under vacuum and layered under diethyl ether. After diffusion at room temperature overnight, a blue precipitate was collected (340 mg, 58% yield over two steps). Crystals suitable for SXRD were grown by layering in acetonitrile under diethyl ether, diffusing at −35 °C, and warming to room temperature. ^1H NMR (CD_2Cl_2, 400 MHz): δ 10.6 (9H, Me-*H*), δ 6.2 (6H, Ph-*H*), 4.4 (3H, Ph-*H*), 1.8 (6H, Ph-*H*). We do not observe a signal from the B-*H* proton by ^1H NMR spectroscopy. $^{19}F\{^1H\}$ NMR (CD_2Cl_2, 400 MHz): δ −1.2. IR (solid, cm^{-1}): 2573 (w, B-*H*). Anal. Calcd for $C_{33}H_{25}BClCoF_9N_6$: C, 50.70; H, 3.22; N, 10.75. Found: C, 47.87; H, 3.19; N, 10.27. The same batch of material passed EA as the dioxygen adduct **2**, so we attribute the low value obtained for C to incomplete combustion of trifluoromethyl groups. The low solubility of **1** prevented characterization by Evans method, although an EPR signal at a high *g*-value is consistent with a high-spin quartet, similar to previously reported triscarbene Co(II)-chloride complexes.[41] This compound is rigorously dried under vacuum to remove residual acetonitrile prior to any further synthetic steps.

In neat acetonitrile or in dichloromethane with a few drops of acetonitrile, **1** changes color from blue to green. The ^1H NMR spectrum of **1** in acetonitrile shows less shifted peaks, and the ^{19}F NMR spectrum is silent. ^1H NMR (CD_3CN, 400 MHz): δ 7.32 (6H, Ph-*H*), 7.24 (3H, Ph-*H*), 6.9 (6H, Ph-*H*), 5.3 (9H, Me-*H*). An EPR spectrum of **1** containing several drops of acetonitrile is consistent with a spin change to $S = 1/2$ (see Figure S20).

Synthesis of 2. 10 mg of **1** was sealed in a septum-capped vial and the vial was sparged with dry O_2 and allowed to react overnight. The excess dioxygen was removed by vacuum, and the material was thereafter handled under an inert atmosphere. No mass was lost during this procedure. $^{18}O_2$-enriched material was synthesized by injection of 6 equiv of enriched oxygen gas instead of sparging. Crystals suitable for SXRD were grown by layering a DCM solution under pentane and diffusing at −35 °C. ^1H NMR (CD_2Cl_2, 400 MHz): δ 7.46 (3H, Ph-*H*), δ 7.18 (4H, Ph-*H*), δ 7.07 (2H, Ph-*H*), δ 6.9 (4H, Ph-*H*), δ 6.82 (2H, Ph-*H*), δ 3.60 (Me-*H*). We do not observe a signal from the B-*H* proton by ^1H NMR spectroscopy, and no signals are observed by $^{19}F\{^1H\}$ NMR spectroscopy. IR (solid, cm^{-1}): 2570 (w, B−H), 1103 (O−O), 416 ($Co−O_2$). Anal. Calcd for $C_{33}H_{25}BClCoF_9N_6$: C, 48.71; H, 3.10; N, 10.33. Found: C, 48.07; H, 3.16; N, 10.07. This compound retains its brown color even after 20 h at 515 μmHg.

Synthesis of 3. A solution of **2** (10 mg, 0.013 mmol) in 5 mL of DCM and a solution of **1** (10 mg, 0.013 mmol) cosolubilized with 2 equiv of $[Na][BAr_4^F]$ (22 mg, 0.026 mmol) in 5 mL of DCM were chilled to −100 °C. The solution of **1** was slowly added to the solution of **2** while stirring vigorously. The reaction was allowed to warm to room temperature, stirred for 10 min, and filtered through Celite. The dark green solution was layered under pentane and allowed to diffuse at −35 °C. Green crystals suitable for SXRD were collected after two nights (26 mg, 62% yield). ^1H NMR (CD_2Cl_2, 400 MHz): δ 9.6 (6H, Ph-*H*), 8.7 (3H, Ph-*H*), 8.5 (3H, Ph-*H*), 7.5 ($[BAr_4^F]^-$), 7.4 ($[BAr_4^F]^-$), 4.2 (9H, Me-*H*). We do not observe a signal from the B-*H* proton by ^1H NMR spectroscopy. $^{19}F\{^1H\}$ NMR (CD_2Cl_2, 400 MHz): δ ∼14 (b), −62 ($[BAr_4^F]^-$). IR (solid, cm^{-1}): 3735 (w, O, H); 2573 (w, B−H). EA and high-resolution mass spectrometry (HRMS) were not possible due to the comparably low stability of the compound.

Synthesis of 4. A solution of **2** (5 mg, 0.0065 mmol) in 5 mL of DCM and a solution of **1** (5 mg, 0.0065 mmol) cosolubilized with 2 equiv of $[Na][BAr_4^F]$ (22 mg, 0.013 mmol) in 5 mL of DCM were chilled to −100 °C. The solution of **1** was slowly added to the solution of **2** while stirring vigorously. The reaction was allowed to warm to room temperature, stirred for 10 min, and chilled back to −100 °C. 2,4-Di-*tert*-butyl-phenol (2.5 mg, 0.013 mmol) was added, and the reaction was again allowed to warm to room temperature, stirred for 10 min, and then filtered through Celite. The dark green solution was layered under pentane and allowed to diffuse at −35 °C. Blue crystals were collected after two nights (16 mg, 76% yield). Crystals suitable for SXRD were collected by vapor diffusion of hexanes into a 1.25 mM solution of **3** in 1,3-difluorobenzene at room temperature overnight. ^{1}H NMR (CD_2Cl_2, 400 MHz): δ 7.7 ($[BAr_4^F]^-$), 8.53 (3H, Ph-*H*), 7.24 (6H, Ph-*H*), 6.91 (6H, Ph-*H*), 3.67 (9H, Me-*H*), 0.25 (1H, O-*H*). We do not observe a signal from the B-*H* proton by ^{1}H NMR spectroscopy. The assignment of the O-*H* resonance was confirmed by exchange with D_2O (Figure S11). $^{19}F\{^1H\}$ NMR (CD_2Cl_2, 400 MHz): δ −56.4 (9F, C*F*$_3$), −62.9 ($[BAr_4^F]^-$). We did not observe a signal from the ligand boron by $^{11}B\{^1H\}$ spectroscopy. IR (solid, cm^{-1}): 3735 (w, O−H), 2573 (w, B−H). We see contamination with residual $[Na][BAr_4^F]$ by ^{1}H and ^{19}F NMR spectroscopies; therefore, EA was not attempted for this compound. HRMS (EI) *m*/*z*. $[M]^{2+}$ calculated for $C_{66}H_{50}B_2Co_2F_{18}N_{12}O_2$: 763.145; found: 763.151.

XAS Data Collection. XAS data collection was performed at the Stanford Synchrotron Radiation Lightsource on beamline 7-3 using an Oxford Helium cryostat at 10 K and collected in fluorescence mode using 30-element solid-state Canberra germanium detectors. Incoming X-rays were detuned to 50% to remove harmonic overtones. Photoreduction was monitored by varying the sample position irradiated for each scan. Data was referenced to Co foil with an edge energy of 7709.3 eV and normalized at 8000 eV. Data was processed with EXAFSPAK.[85] Derivative spectra were regularized to minimize noise (TVDiff).[86]

The Co K-edge XAS spectrum of **1** was obtained as a solid dispersed in dextrose. The Co K-edge XAS spectra of **2** and **3** were collected as 2.5 mM [Co] 1,2-difluorobenzene frozen solutions. The sample of **3** was prepared following the same procedure as above except at −50 °C in 1,2-difluorobenzene instead of at −100 °C in dichloromethane, and it was not allowed to warm to room temperature. This sample was immediately frozen and stored cold prior to data collection.

EXAFS fitting was performed by first fitting with amplitudes and phases computed by EXAFSPAK. We found that the best fit was obtained with five identical first-sphere scatters, one heavy Co−Co scatterer, and three second-sphere scatterers. Splitting the first sphere into two shorter oxygen scatterers and three longer carbon scatterers, addition of a second-sphere fluorine scatterer, replacement of the Co−Co scatterer with a Co−Cl scatterer, and removal of the second-sphere scatterers and/or the Co−Co scatterer all resulted in either an unphysical Debye−Waller factor or a substantially worse fit. A structure of **3** with the primary-sphere and Co−Co distances constrained to those of the best fit from EXAFSPAK was generated using one-iteration geometry optimization and was used to computed amplitudes and phases with FEFF8.[87] We used these amplitudes and phases to calculate a final fit for the EXAFS data; this fit included all unique scattering pathways but constrained the ones that were unresolvable by EXAFSPAK to have the same final scattering distance and Debye−Waller factor. We found that the secondary sphere could be explained with the three boron-binding nitrogens adjacent to the cobalt-binding carbons; while they were not constrained to the exact distances found by EXAFSPAK, they were each within the expected resolution of the fit.

XRD Structure Determination. The diffraction data for the initial product formed during the synthesis of **1** were measured at the Advanced Photon Source of Argonne National Laboratory (beamline 15-ID B,C,D) using X-ray radiation with a wavelength of λ = 0.41328 Å. The diffraction data for **1** and **4** were measured at 100 K on a Bruker D8 VENTURE with PHOTON 100 CMOS detector system equipped with a Mo-target microfocus X-ray tube (λ = 0.71073 Å). The diffraction data for **3** were measured at 100 K on a Bruker D8 VENTURE diffractometer equipped with a microfocus Mo-target X-ray tube (λ = 0.71073 Å) and a PHOTON II Charge-Integrating Pixel Array Detector (CPAD). Data reduction and integration were performed with the Bruker APEX4 software package (Bruker AXS, version 2021.4−0, 2021). Data for all structures were scaled and corrected for absorption effects using the multiscan procedure as implemented in SADABS (Bruker AXS, version 2016/2, part of Bruker APEX4 software package). The diffraction data for **2** were measured at 100 K on an XtalAB Synergy-S dual-source single-crystal X-ray diffractometer using a PhotonJet-S Cu 50 W Microfocus X-ray source (λ = 1.54184 Å) and a HyPix-6000HE Hybrid Photon Counting detector. Data reduction and integration for **2** were performed with the CrysAlisPro 1.171.43.75a (Rigaku Oxford Diffraction, 2023) software package, with numerical absorption correction based on Gaussian integration over a multifaceted crystal model and empirical absorption correction using spherical harmonics, implemented in the SCALE3 ABSPACK scaling algorithm.

All structures were solved by the dual method implemented in SHELXT (version 2018/2) and refined by a full-matrix least-squares procedure using OLEX2 software package (SHELXL refinement program version 2019/3).[88−90] C−H hydrogen atoms were generated by geometrical considerations and allowed to ride on their carrier atoms with an isotropic displacement parameter related to the equivalent displacement parameter of their carrier atoms. Structure **1** was refined as a two-component twin crystal. Several phenyl rings were found to be rotationally disordered. The Cl atom was also disordered over two positions. The structure of **3** contains a mask over a disordered solvent region in the crystal; while we could not resolve this disorder, electron count and void volumes consist of molecules of dichloromethane or pentane or a mixture of both.

The structure of **2** shows an interesting cofacial orientation of Cl and O_2 ligands attached to Co. Initial refinement of the Cl and O_2 ligands as fully occupied revealed some small residual electron densities at two positions at the same distances as the position of the Cl atom from Co. These were assigned to Cl atoms of two other minor isomers with different orientations of Cl and O_2 ligands. The occupancies of all three Cl atoms were refined but constrained to be equal to unity (SUMP command in SHELXL: SUMP 1 0.001 1 2 1 3 1 4). This led to refined occupancies as 89.7, 6.7, and 3.6%. At the final refinement steps, the occupancies of the O_2 ligand were adjusted to be the same as for the refined occupancy of the Cl atom in the major isomer. Reliably finding minor orientations of O_2 ligands with such small occupancies was problematic, and so only a major orientation of O_2 was used in the final structure (Figure S33). We note that crystal packing is the most probable reason for the high preference for a particular Cl and O_2 orientation in the solid-state structure of **2**. The crystal contains extra cocrystallized dichloromethane molecules, which are involved in the crystal packing beyond simple pore-filling. Two DCM molecules form intermolecular hydrogen bonds connecting two complexes with $C(Cl_2)-H\cdots Cl(Co)$ distances ranging from 2.57 to 2.77 Å (C atoms in CH_2Cl_2 to Cl(Co) distances range from 3.481(15) to 3.635(15) Å, Figure S34). This crystal packing is putatively most favorable for only one of the isomers.

The hydrogen atom attached to oxygen in **4** is visible in the difference Fourier map and can be freely refined without using any geometric or thermal parameter restraints. This is not the case for compound **3**. In contrast, the largest residual electron density in the vicinity of oxygen is less than 0.3 e·Å^{-3}, and attempts to refine it as a H atom were not successful. Importantly, the geometric parameters of the Co_2O_2 core change on going from **3** to **4** (Table S6). We should note that the situation where a small submixture of a cocrystallized hydroperoxide formed, for example, due to a small degradation during the slow process of crystal growth, cannot be fully excluded. In such a case, that would lead to apparent elongation of the Co−Co distance observed in **3**. In any case, probing the existence of a proton that is only partially occupied and attached to a heteroatom can hardly be conclusive from the X-ray diffraction experiment only, and so a range of other analytic methods were utilized to address the issue of the Co oxidation state in **3** and **4**.

DFT Calculations. All DFT calculations were performed in the ORCA 5.0.2 software suite using the TPSSh functional with the resolution of identity and chain of spheres approximations, the D3 dispersion correction with Becke−Johnson damping, and a solvent correction using the conductor-like polarizable continuum model with the dielectric properties of dichloromethane.[91−93] The cobalt center was given the def-TZVPP basis set, all atoms bound to the cobalt center were given the def2-TZVP basis set, and all other atoms were given the def2-SV(P) basis set.[94,95] Geometries were optimized using the default convergence criterion and numerical frequency to confirm convergence to a stable minimum and predict the IR spectra. There was one spurious imaginary frequency found in the frequency calculation of **4** that was delocalized throughout the entire molecule. It was used as the absolute value for thermochemistry calculations. Free energies were computed using the quasi-RRHO approximation of Grimme and co-workers with a standard temperature of 296 K and a standard concentration of 1 M for solution species and 1 atm for gaseous species.[96] Optimized structures are included in the Supporting Information as xyz files.

Percent buried volume was determined using the online SambVca application with the sphere centered on an oxygen atom and the negative *z*-axis going defined by the second oxygen atom.[83] We removed the center oxygen atom, used scaled bondi radii, included hydrogens, and had a sphere radius of 3.5 Å.

■ ASSOCIATED CONTENT

Supporting Information

The Supporting Information is available free of charge at https://pubs.acs.org/doi/10.1021/jacs.4c07335.

Spectroscopic data, cyclic voltammograms, crystallographic details, and DFT-optimized geometries (PDF)

xyz files (ZIP)

Accession Codes

CCDC 2359144−2359148 contain the supporting crystallographic data for this paper. These data can be obtained free of charge via www.ccdc.cam.ac.uk/data_request/cif, or by emailing data_request@ccdc.cam.ac.uk, or by contacting The Cambridge Crystallographic Data Centre, 12 Union Road, Cambridge CB2 1EZ, U.K.; fax: +44 1223 336033.

■ AUTHOR INFORMATION

Corresponding Author

John S. Anderson − *Department of Chemistry, The University of Chicago, Chicago, Illinois 60637, United States;* orcid.org/0000-0002-0730-3018; Email: jsanderson@uchicago.edu

Authors

Joseph E. Schneider − *Department of Chemistry, The University of Chicago, Chicago, Illinois 60637, United States*

Shilin Zeng − *Department of Chemistry, The University of Chicago, Chicago, Illinois 60637, United States*

Sophie W. Anferov − *Department of Chemistry, The University of Chicago, Chicago, Illinois 60637, United States;* orcid.org/0000-0003-3972-5845

Alexander S. Filatov − *Department of Chemistry, The University of Chicago, Chicago, Illinois 60637, United States;* orcid.org/0000-0002-8378-1994

Complete contact information is available at: https://pubs.acs.org/10.1021/jacs.4c07335

Notes

The authors declare no competing financial interest.

■ ACKNOWLEDGMENTS

This work was supported by the National Science Foundation (#2348761) and the NIGMS (R35 GM133470). J.E.S. thanks the U.S. Department of Defense for a National Defense Science and Engineering Graduate Fellowship (00003765), and J.S.A. thanks the Dreyfus Foundation for a Teacher-Scholar Award (TC-21-064). The authors thank Dr. Pat Crossland for assistance with XAS data collection and workup, Joe Scott and Maia Czaikowski for assistance collecting vibrational spectroscopy, and Dr. Josh Kurutz for assistance with DOSY spectroscopy. The authors also thank Professor Graham George for his assistance in using his EXAFSPAK software suite. This work made use of the IMSERC Crystallography facility at Northwestern University, which has received support from the Soft and Hybrid Nanotechnology Experimental (SHyNE) Resource (NSF ECCS-2025633), Northwestern University. The authors also thank Charlotte Stern and Dr. Christos D. Malliakas for their assistance with SXRD acquisition at IMSERC. Some data reported here was collected at ChemMatCARS Sector 15 that is supported by the NSF under Grant Number NSF/CHE-1834750. This research used resources of the APS, a U.S. DOE Office of Science User Facility operated for the DOE Office of Science by the Argonne National Laboratory under Contract No. DE-AC02-06CH11357. The authors thank Dr. Yu-Sheng Chen for assistance with SXRD acquisition at 15-ID-B,C,D. Use of the Stanford Synchrotron Radiation Lightsource, SLAC National Accelerator Laboratory, is supported by the U.S. Department of Energy, Office of Science, Office of Basic Energy Sciences under Contract No. DE-AC02-76SF00515. The SSRL Structural Molecular Biology Program is supported by the DOE Office of Biological and Environmental Research, and by the National Institutes of Health, National Institute of General Medical Sciences (P30GM133894). The contents of this publication are solely the responsibility of the authors and do not necessarily represent the official views of NIGMS or NIH. The results reported in this manuscript have been adapted from a thesis.

■ REFERENCES

(1) Singh, A.; Spiccia, L. Water Oxidation Catalysts Based on Abundant 1st Row Transition Metals. *Coord. Chem. Rev.* **2013**, *257* (17), 2607−2622.

(2) Kärkäs, M. D.; Verho, O.; Johnston, E. V.; Åkermark, B. Artificial Photosynthesis: Molecular Systems for Catalytic Water Oxidation. *Chem. Rev.* **2014**, *114* (24), 11863−12001.

(3) Smith, P. F.; Hunt, L.; Laursen, A. B.; Sagar, V.; Kaushik, S.; Calvinho, K. U. D.; Marotta, G.; Mosconi, E.; De Angelis, F.; Dismukes, G. C. Water Oxidation by the [Co4O4(OAc)4(Py)4]+ Cubium Is Initiated by OH− Addition. *J. Am. Chem. Soc.* **2015**, *137* (49), 15460−15468.

(4) Amtawong, J.; Nguyen, A. I.; Tilley, T. D. Mechanistic Aspects of Cobalt−Oxo Cubane Clusters in Oxidation Chemistry. *J. Am. Chem. Soc.* **2022**, *144* (4), 1475−1492.

(5) Wu, Q.; Zhang, B.; Lu, Y. Progress and Perspective of High-Voltage Lithium Cobalt Oxide in Lithium-Ion Batteries. *J. Energy Chem.* **2022**, *74*, 283−308.

(6) Lewis, N. S.; Nocera, D. G. Powering the Planet: Chemical Challenges in Solar Energy Utilization. *Proc. Natl. Acad. Sci. U.S.A.* **2006**, *103* (43), 15729−15735.

(7) Yin, Q.; Tan, J. M.; Besson, C.; Geletii, Y. V.; Musaev, D. G.; Kuznetsov, A. E.; Luo, Z.; Hardcastle, K. I.; Hill, C. L. A Fast Soluble Carbon-Free Molecular Water Oxidation Catalyst Based on Abundant Metals. *Science* **2010**, *328* (5976), 342−345.

(8) Costentin, C.; Nocera, D. G. Self-Healing Catalysis in Water. *Proc. Natl. Acad. Sci. U.S.A.* **2017**, *114* (51), 13380−13384.

(9) Wang, L.-P.; Van Voorhis, T. Direct-Coupling O2 Bond Forming a Pathway in Cobalt Oxide Water Oxidation Catalysts. *J. Phys. Chem. Lett.* **2011**, *2* (17), 2200−2204.

(10) Bajdich, M.; García-Mota, M.; Vojvodic, A.; Nørskov, J. K.; Bell, A. T. Theoretical Investigation of the Activity of Cobalt Oxides for the Electrochemical Oxidation of Water. *J. Am. Chem. Soc.* **2013**, *135* (36), 13521−13530.

(11) Li, X.; Siegbahn, P. E. M. Water Oxidation Mechanism for Synthetic Co−Oxides with Small Nuclearity. *J. Am. Chem. Soc.* **2013**, *135* (37), 13804−13813.

(12) Zhang, M.; de Respinis, M.; Frei, H. Time-Resolved Observations of Water Oxidation Intermediates on a Cobalt Oxide Nanoparticle Catalyst. *Nat. Chem.* **2014**, *6* (4), 362−367.

(13) Lin, Y.; Yu, L.; Tang, L.; Song, F.; Schlögl, R.; Heumann, S. In Situ Identification and Time-Resolved Observation of the Interfacial State and Reactive Intermediates on a Cobalt Oxide Nanocatalyst for the Oxygen Evolution Reaction. *ACS Catal.* **2022**, *12* (9), 5345−5355.

(14) Moysiadou, A.; Lee, S.; Hsu, C.-S.; Chen, H. M.; Hu, X. Mechanism of Oxygen Evolution Catalyzed by Cobalt Oxyhydroxide: Cobalt Superoxide Species as a Key Intermediate and Dioxygen Release as a Rate-Determining Step. *J. Am. Chem. Soc.* **2020**, *142* (27), 11901−11914.

(15) Nurdin, L.; Spasyuk, D. M.; Fairburn, L.; Piers, W. E.; Maron, L. Oxygen−Oxygen Bond Cleavage and Formation in Co(II)-Mediated Stoichiometric O2 Reduction via the Potential Intermediacy of a Co(IV) Oxyl Radical. *J. Am. Chem. Soc.* **2018**, *140* (47), 16094−16105.

(16) Zhang, L.; Liu, Y.; Deng, L. Three-Coordinate Cobalt(IV) and Cobalt(V) Imido Complexes with N-Heterocyclic Carbene Ligation: Synthesis, Structure, and Their Distinct Reactivity in C−H Bond Amination. *J. Am. Chem. Soc.* **2014**, *136* (44), 15525−15528.

(17) Mao, W.; Fehn, D.; Heinemann, F. W.; Scheurer, A.; Munz, D.; Meyer, K. A Pair of Cobalt(III/IV) Terminal Imido Complexes. *Angew. Chem., Int. Ed.* **2021**, *60* (30), 16480−16486.

(18) Mao, W.; Zhang, Z.; Fehn, D.; Jannuzzi, S. A. V.; Heinemann, F. W.; Scheurer, A.; van Gastel, M.; DeBeer, S.; Munz, D.; Meyer, K. Synthesis and Reactivity of a Cobalt-Supported Singlet Nitrene. *J. Am. Chem. Soc.* **2023**, *145* (25), 13650−13662.

(19) Yang, J.; Tripodi, G. L.; Derks, M. T. G. M.; Seo, M. S.; Lee, Y.-M.; Southwell, K. W.; Shearer, J.; Roithová, J.; Nam, W. Generation, Spectroscopic Characterization, and Computational Analysis of a Six-Coordinate Cobalt(III)-Imidyl Complex with an Unusual S = 3/2 Ground State That Promotes N-Group and Hydrogen Atom-Transfer Reactions with Exogenous Substrates. *J. Am. Chem. Soc.* **2023**, *145* (48), 26106−26121.

(20) Sykes, A. G.; Weil, J. A. The Formation, Structure, and Reactions of Binuclear Complexes of Cobalt. In *Progress in Inorganic Chemistry*; John Wiley & Sons, Ltd., 1970; pp 1−106.

(21) Jones, R. D.; Summerville, D. A.; Basolo. Fred. Synthetic Oxygen Carriers Related to Biological Systems. *Chem. Rev.* **1979**, *79* (2), 139−179.

(22) Wang, C.-C.; Chang, H.-C.; Lai, Y.-C.; Fang, H.; Li, C.-C.; Hsu, H.-K.; Li, Z.-Y.; Lin, T.-S.; Kuo, T.-S.; Neese, F.; Ye, S.; Chiang, Y.-W.; Tsai, M.-L.; Liaw, W.-F.; Lee, W.-Z. A Structurally Characterized Nonheme Cobalt−Hydroperoxo Complex Derived from Its Superoxo Intermediate via Hydrogen Atom Abstraction. *J. Am. Chem. Soc.* **2016**, *138* (43), 14186−14189.

(23) Corona, T.; Padamati, S. K.; Acuña-Parés, F.; Duboc, C.; Browne, W. R.; Company, A. Trapping of Superoxido Cobalt and Peroxido Dicobalt Species Formed Reversibly from CoII and O2. *Chem. Commun.* **2017**, *53* (86), 11782−11785.

(24) Gordon, J. B.; Vilbert, A. C.; Siegler, M. A.; Lancaster, K. M.; Moënne-Loccoz, P.; Goldberg, D. P. A Nonheme Thiolate-Ligated Cobalt Superoxo Complex: Synthesis and Spectroscopic Characterization, Computational Studies, and Hydrogen Atom Abstraction Reactivity. *J. Am. Chem. Soc.* **2019**, *141* (8), 3641−3653.

(25) Malik, D. D.; Chandra, A.; Sook Seo, M.; Lee, Y.-M.; R Farquhar, E.; Mebs, S.; Dau, H.; Ray, K.; Nam, W. Formation of Cobalt−Oxygen Intermediates by Dioxygen Activation at a Mononuclear Nonheme Cobalt(Ii) Center. *Dalton Trans.* **2021**, *50* (34), 11889−11898.

(26) Nguyen, A. I.; Hadt, R. G.; Solomon, E. I.; Tilley, T. D. Efficient C−H Bond Activations via O2 Cleavage by a Dianionic Cobalt(Ii) Complex. *Chem. Sci.* **2014**, *5* (7), 2874−2878.

(27) Kodera, M.; Kawahara, Y.; Hitomi, Y.; Nomura, T.; Ogura, T.; Kobayashi, Y. Reversible O−O Bond Scission of Peroxodiiron(III) to High-Spin Oxodiiron(IV) in Dioxygen Activation of a Diiron Center with a Bis-Tpa Dinucleating Ligand as a Soluble Methane Monooxygenase Model. *J. Am. Chem. Soc.* **2012**, *134* (32), 13236−13239.

(28) Jasniewski, A. J.; Que, L. Dioxygen Activation by Nonheme Diiron Enzymes: Diverse Dioxygen Adducts, High-Valent Intermediates, and Related Model Complexes. *Chem. Rev.* **2018**, *118* (5), 2554−2592.

(29) Banerjee, S.; Draksharapu, A.; Crossland, P. M.; Fan, R.; Guo, Y.; Swart, M.; Que, L., Jr. Sc3+-Promoted O−O Bond Cleavage of a (*μ*-1,2-Peroxo)Diiron(III) Species Formed from an Iron(II) Precursor and O2 to Generate a Complex with an FeIV2(*μ*-O)2 Core. *J. Am. Chem. Soc.* **2020**, *142* (9), 4285−4297.

(30) Cho, Y. I.; Joseph, D. M.; Rose, M. J. Criss-Crossed" Dinucleating Behavior of an N4 Schiff Base Ligand: Formation of a *μ*-OH,*μ*-O2 Dicobalt(III) Core via O2 Activation. *Inorg. Chem.* **2013**, *52* (23), 13298−13300.

(31) Wang, H.-Y.; Mijangos, E.; Ott, S.; Thapper, A. Water Oxidation Catalyzed by a Dinuclear Cobalt−Polypyridine Complex. *Angew. Chem., Int. Ed.* **2014**, *53* (52), 14499−14502.

(32) Kotani, H.; Hong, D.; Satonaka, K.; Ishizuka, T.; Kojima, T. Mechanistic Insight into Dioxygen Evolution from Diastereomeric *μ*-Peroxo Dinuclear Co(III) Complexes Based on Stoichiometric Electron-Transfer Oxidation. *Inorg. Chem.* **2019**, *58* (6), 3676−3682.

(33) Depenbrock, F.; Limpke, T.; Bill, E.; SantaLucia, D. J.; van Gastel, M.; Walleck, S.; Oldengott, J.; Stammler, A.; Bögge, H.; Glaser, T. Reactivities and Electronic Structures of *μ*-1,2-Peroxo and *μ*-1,2-Superoxo CoIIICoIII Complexes: Electrophilic Reactivity and O2 Release Induced by Oxidation. *Inorg. Chem.* **2023**, *62* (43), 17913−17930.

(34) Dimitrou, K.; Brown, A. D.; Concolino, T. E.; Rheingold, A. L.; Christou, G. Mixed-Valence, Tetranuclearcobalt(III,IV) Complexes: Preparation and Propertiesof[Co4O4(O2CR)2(Bpy)4]3+ Salts. *Chem. Commun.* **2001**, No. 14, 1284−1285.

(35) McAlpin, J. G.; Stich, T. A.; Ohlin, C. A.; Surendranath, Y.; Nocera, D. G.; Casey, W. H.; Britt, R. D. Electronic Structure Description of a [Co(III)3Co(IV)O4] Cluster: A Model for the Paramagnetic Intermediate in Cobalt-Catalyzed Water Oxidation. *J. Am. Chem. Soc.* **2011**, *133* (39), 15444−15452.

(36) Brodsky, C. N.; Hadt, R. G.; Hayes, D.; Reinhart, B. J.; Li, N.; Chen, L. X.; Nocera, D. G. In Situ Characterization of Cofacial Co(IV) Centers in Co4O4 Cubane: Modeling the High-Valent Active Site in Oxygen-Evolving Catalysts. *Proc. Natl. Acad. Sci. U.S.A.* **2017**, *114* (15), 3855−3860.

(37) Ezhov, R.; Ravari, A. K.; Bury, G.; Smith, P. F.; Pushkar, Y. Do Multinuclear 3d Metal Catalysts Achieve O−O Bond Formation via Radical Coupling or via Water Nucleophilic Attack? WNA Leads the Way in [Co4O4]N+. *Chem. Catal.* **2021**, *1* (2), 407−422.

(38) Nguyen, A. I.; Van Allsburg, K. M.; Terban, M. W.; Bajdich, M.; Oktawiec, J.; Amtawong, J.; Ziegler, M. S.; Dombrowski, J. P.; Lakshmi, K. V.; Drisdell, W. S.; Yano, J.; Billinge, S. J. L.; Tilley, T. D. Stabilization of Reactive Co4O4 Cubane Oxygen-Evolution Catalysts within Porous Frameworks. *Proc. Natl. Acad. Sci. U.S.A.* **2019**, *116* (24), 11630−11639.

(39) Wang, B.; Lee, Y.-M.; Tcho, W.-Y.; Tussupbayev, S.; Kim, S.-T.; Kim, Y.; Seo, M. S.; Cho, K.-B.; Dede, Y.; Keegan, B. C.; Ogura, T.; Kim, S. H.; Ohta, T.; Baik, M.-H.; Ray, K.; Shearer, J.; Nam, W. Synthesis and Reactivity of a Mononuclear Non-Haem Cobalt(IV)-Oxo Complex. *Nat. Commun.* **2017**, *8*, No. 14839.

(40) Yang, J.; Dong, H. T.; Seo, M. S.; Larson, V. A.; Lee, Y.-M.; Shearer, J.; Lehnert, N.; Nam, W. The Oxo-Wall Remains Intact: A Tetrahedrally Distorted Co(IV)−Oxo Complex. *J. Am. Chem. Soc.* **2021**, *143* (41), 16943−16959.

(41) Goetz, M. K.; Schneider, J. E.; Filatov, A. S.; Jesse, K. A.; Anderson, J. S. Enzyme-Like Hydroxylation of Aliphatic C−H Bonds From an Isolable Co-Oxo Complex. *J. Am. Chem. Soc.* **2021**, *143* (49), 20849−20862.

(42) Li, Y.; Handunneththige, S.; Farquhar, E. R.; Guo, Y.; Talipov, M. R.; Li, F.; Wang, D. Highly Reactive CoIII,IV2(μ-O)2 Diamond Core Complex That Cleaves C−H Bonds. *J. Am. Chem. Soc.* **2019**, *141* (51), 20127−20136.

(43) Li, Y.; Abelson, C.; Que, L.; Wang, D. 106-Fold Faster C−H Bond Hydroxylation by a CoIII,IV2(μ-O)2 Complex [via a CoIII2(μ-O)(μ-OH) Intermediate] versus Its FeIIIFeIV Analog. *Proc. Natl. Acad. Sci. U.S.A.* **2023**, *120* (51), No. e2307950120.

(44) Thorarinsdottir, A. E.; Nocera, D. G. Energy Catalysis Needs Ligands with High Oxidative Stability. *Chem. Catal.* **2021**, *1* (1), 32−43.

(45) Reinaud, O. M.; Theopold, K. H. Hydrogen Tunneling in the Activation of Dioxygen by a Tris(Pyrazolyl)Borate Cobalt Complex. *J. Am. Chem. Soc.* **1994**, *116* (15), 6979−6980.

(46) Scott, J. S.; Schneider, J. E.; Tewelde, E. G.; Gardner, J. G.; Anferov, S. W.; Filatov, A. S.; Anderson, J. S. Combining Donor Strength and Oxidative Stability in Scorpionates: A Strongly Donating Fluorinated Mesoionic Tris(Imidazol-5-Ylidene)Borate Ligand. *Inorg. Chem.* **2023**, *62* (51), 21224−21232.

(47) Le Mest, Y.; Inisan, C.; Laouénan, A.; L'Her, M.; Talarmin, J.; El Khalifa, M.; Saillard, J.-Y. Reactivity toward Dioxygen of Dicobalt Face-to-Face Diporphyrins in Aprotic Media. Experimental and Theoretical Aspects. Possible Mechanistic Implication in the Reduction of Dioxygen. *J. Am. Chem. Soc.* **1997**, *119* (26), 6095−6106.

(48) Fukuzumi, S.; Okamoto, K.; Gros, C. P.; Guilard, R. Mechanism of Four-Electron Reduction of Dioxygen to Water by Ferrocene Derivatives in the Presence of Perchloric Acid in Benzonitrile, Catalyzed by Cofacial Dicobalt Porphyrins. *J. Am. Chem. Soc.* **2004**, *126* (33), 10441−10449.

(49) Givaja, G.; Volpe, M.; Edwards, M. A.; Blake, A. J.; Wilson, C.; Schröder, M.; Love, J. B. Dioxygen Reduction at Dicobalt Complexes of a Schiff Base Calixpyrrole Ligand. *Angew. Chem., Int. Ed.* **2007**, *46* (4), 584−586.

(50) Rosenthal, J.; Nocera, D. G. Role of Proton-Coupled Electron Transfer in O−O Bond Activation. *Acc. Chem. Res.* **2007**, *40* (7), 543−553.

(51) Oddon, F.; Chiba, Y.; Nakazawa, J.; Ohta, T.; Ogura, T.; Hikichi, S. Characterization of Mononuclear Non-Heme Iron(III)-Superoxo Complex with a Five-Azole Ligand Set. *Angew. Chem., Int. Ed.* **2015**, *54* (25), 7336−7339.

(52) Hoffman, B. M.; Diemente, D. L.; Basolo, F. Electron Paramagnetic Resonance Studies of Some Cobalt(II) Schiff Base Compounds and Their Monomeric Oxygen Adducts. *J. Am. Chem. Soc.* **1970**, *92* (1), 61−65.

(53) Diemente, D.; Hoffman, B. M.; Basolo, F. Electron Spin Resonance Studies of 1:1 Cobalt−Oxygen Adducts. *J. Chem. Soc. D* **1970**, *0* (8), 467−468.

(54) Rodley, G. A.; Robinson, W. T. Structure of a Monomeric Oxygen-Carrying Complex. *Nature* **1972**, *235* (5339), 438−439.

(55) Egan, J. W., Jr.; Haggerty, B. S.; Rheingold, A. L.; Sendlinger, S. C.; Theopold, K. H. Crystal Structure of a Side-on Superoxo Complex of Cobalt and Hydrogen Abstraction by a Reactive Terminal Oxo Ligand. *J. Am. Chem. Soc.* **1990**, *112* (6), 2445−2446.

(56) Hu, X.; Castro-Rodriguez, I.; Meyer, K. Dioxygen Activation by a Low-Valent Cobalt Complex Employing a Flexible Tripodal N-Heterocyclic Carbene Ligand. *J. Am. Chem. Soc.* **2004**, *126* (41), 13464−13473.

(57) Noh, H.; Jeong, D.; Ohta, T.; Ogura, T.; Valentine, J. S.; Cho, J. Distinct Reactivity of a Mononuclear Peroxocobalt(III) Species toward Activation of Nitriles. *J. Am. Chem. Soc.* **2017**, *139* (32), 10960−10963.

(58) DeRosha, D. E.; Mercado, B. Q.; Lukat-Rodgers, G.; Rodgers, K. R.; Holland, P. L. Enhancement of C−H Oxidizing Ability in Co−O2 Complexes through an Isolated Heterobimetallic Oxo Intermediate. *Angew. Chem., Int. Ed.* **2017**, *56* (12), 3211−3215.

(59) Terry, N. W. I.; Amma, E. L.; Vaska, L. Molecular Oxygen Binding in a Monomeric Cobalt Complex. Crystal and Molecular Structure of Dioxygen-Bis[Cis-1,2-Bis(Diphenylphosphino)-Ethylene]Cobalt Tetrafluoroborate. *J. Am. Chem. Soc.* **1972**, *94* (2), 653−655.

(60) Halpern, J.; Goodall, B. L.; Khare, G. P.; Lim, H. S.; Pluth, J. J. Reaction of Oxygen with Dicyanotris(Dimethylphenylphosphine)-Cobalt(II). Synthesis, Structure, and Reactivity of a Novel Cobalt-Dioxygen Adduct. *J. Am. Chem. Soc.* **1975**, *97* (8), 2301−2303.

(61) Cho, J.; Sarangi, R.; Kang, H. Y.; Lee, J. Y.; Kubo, M.; Ogura, T.; Solomon, E. I.; Nam, W. Synthesis, Structural, and Spectroscopic Characterization and Reactivities of Mononuclear Cobalt(III)−Peroxo Complexes. *J. Am. Chem. Soc.* **2010**, *132* (47), 16977−16986.

(62) Rahman, A. F. M. M.; Jackson, W. G.; Willis, A. C. The First Sideways-Bonded Peroxo Complex for a Tetraaminecobalt(III) Species. *Inorg. Chem.* **2004**, *43* (24), 7558−7560.

(63) Li, Y.; Handunneththige, S.; He, W.; Talipov, M. R.; Wang, D. A Co(III)-Peroxo-Arylboronate Complex Formed by Nucleophilic Reaction of a Co(III)-Peroxo Species. *J. Inorg. Biochem.* **2024**, *256*, No. 112552.

(64) Maki, A. H.; Edelstein, N.; Davison, A.; Holm, R. H. Electron Paramagnetic Resonance Studies of the Electronic Structures of Bis(Maleonitriledithiolato)Copper(II), -Nickel(III), -Cobalt(II), and -Rhodium(II) Complexes. *J. Am. Chem. Soc.* **1964**, *86* (21), 4580−4587.

(65) Topich, J.; Halpern, J. Organobis(Dioximato)Cobalt(IV) Complexes: Electron Paramagnetic Resonance Spectra and Electronic Structures. *Inorg. Chem.* **1979**, *18* (5), 1339−1343.

(66) Urban, M. W.; Nonaka, Y.; Nakamoto, K. Infrared and Resonance Raman Spectra of Molecular Oxygen Adducts of [N,N'-Ethylenebis(Acetylacetoniminato)]Cobalt(II). *Inorg. Chem.* **1982**, *21* (3), 1046−1049.

(67) Bajdor, K.; Nakamoto, K.; Kanatomi, H.; Murase, I. Resonance Raman Spectra of Molecular Oxygen Adducts of Co(Salen) and Its Derivatives in Solution. *Inorg. Chim. Acta* **1984**, *82* (2), 207−210.

(68) Green, M. T. Application of Badger's Rule to Heme and Non-Heme Iron−Oxygen Bonds: An Examination of Ferryl Protonation States. *J. Am. Chem. Soc.* **2006**, *128* (6), 1902−1906.

(69) Spaeth, A. D.; Gagnon, N. L.; Dhar, D.; Yee, G. M.; Tolman, W. B. Determination of the Cu(III)−OH Bond Distance by Resonance Raman Spectroscopy Using a Normalized Version of Badger's Rule. *J. Am. Chem. Soc.* **2017**, *139* (12), 4477−4485.

(70) Carter, M. J.; Rillema, D. P.; Basolo, F. Oxygen Carrier and Redox Properties of Some Neutral Cobalt Chelates. Axial and in-Plane Ligand Effects. *J. Am. Chem. Soc.* **1974**, *96* (2), 392−400.

(71) Cramer, C. J.; Tolman, W. B.; Theopold, K. H.; Rheingold, A. L. Variable Character of O−O and M−O Bonding in Side-on (H2) 1:1 Metal Complexes of O2. *Proc. Natl. Acad. Sci. U.S.A.* **2003**, *100* (7), 3635−3640.

(72) Bott, G.; Field, L. D.; Sternhell, S. Steric Effects. A Study of a Rationally Designed System. *J. Am. Chem. Soc.* **1980**, *102* (17), 5618−5626.

(73) Belot, V.; Farran, D.; Jean, M.; Albalat, M.; Vanthuyne, N.; Roussel, C. Steric Scale of Common Substituents from Rotational Barriers of N-(o-Substituted Aryl)Thiazoline-2-Thione Atropisomers. *J. Org. Chem.* **2017**, *82* (19), 10188−10200.

(74) Goodenough, J. B. Theory of the Role of Covalence in the Perovskite-Type Manganites [La,M(II)]MnO3]. *Phys. Rev.* **1955**, *100* (2), No. 564.

(75) Kanamori, J. Theory of the Magnetic Properties of Ferrous and Cobaltous Oxides, I. *Prog. Theor. Phys.* **1957**, *17* (2), 177−196.

(76) Anderson, P. W. New Approach to the Theory of Superexchange Interactions. *Phys. Rev.* **1959**, *115* (1), 2−13.

(77) DeLucia, A. A.; Kelly, K. A.; Herrera, K. A.; Gray, D. L.; Olshansky, L. Intramolecular Hydrogen-Bond Interactions Tune Reactivity in Biomimetic Bis(μ-Hydroxo)Dicobalt Complexes. *Inorg. Chem.* **2021**, *60* (20), 15599−15609.

(78) DeLucia, A. A.; Olshansky, L. Carboxylate Shift Dynamics in Biomimetic Co2(μ−OH)2 Complexes. *Inorg. Chem.* **2024**, *63* (2), 1109−1118.

(79) Westre, T. E.; Kennepohl, P.; DeWitt, J. G.; Hedman, B.; Hodgson, K. O.; Solomon, E. I. A Multiplet Analysis of Fe K-Edge 1s

→ 3d Pre-Edge Features of Iron Complexes. *J. Am. Chem. Soc.* **1997**, *119* (27), 6297−6314.

(80) Luo, Y.-R. *Handbook of Bond Dissociation Energies in Organic Compounds*; CRC Press: Boca Raton, 2003.

(81) Mayer, J. M. Simple Marcus-Theory-Type Model for Hydrogen-Atom Transfer/Proton-Coupled Electron Transfer. *J. Phys. Chem. Lett.* **2011**, *2* (12), 1481−1489.

(82) Klein, J. E. M. N.; Dereli, B.; Que, L.; Cramer, C. J. Why Metal−Oxos React with Dihydroanthracene and Cyclohexadiene at Comparable Rates, despite Having Different C−H Bond Strengths. A Computational Study. *Chem. Commun.* **2016**, *52* (69), 10509−10512.

(83) Poater, A.; Cosenza, B.; Correa, A.; Giudice, S.; Ragone, F.; Scarano, V.; Cavallo, L. Samb*V*ca: A Web Application for the Calculation of the Buried Volume of N-Heterocyclic Carbene Ligands. *Chem. - Eur. J.* **2009**, *2009* (13), 1759−1766.

(84) Rein, S.; Lewe, P.; Andrade, S. L.; Kacprzak, S.; Weber, S. Global Analysis of Complex PELDOR Time Traces. *J. Magn. Reson.* **2018**, *295*, 17−26.

(85) George, G. N. EXAFSPAK, 2000. https://www-ssrl.slac.stanford.edu/~george/exafspak/exafs.htmhttps://www-ssrl.slac.stanford.edu/~george/exafspak/exafs.htm.

(86) Chartrand, R. Numerical Differentiation of Noisy, Nonsmooth Data. *ISRN Appl. Math.* **2011**, *2011*, No. 164564.

(87) Ankudinov, A. L.; Ravel, B.; Rehr, J. J.; Conradson, S. D. Real-Space Multiple-Scattering Calculation and Interpretation of x-Ray-Absorption near-Edge Structure. *Phys. Rev. B* **1998**, *58* (12), No. 7565.

(88) Sheldrick, G. M. A Short History of SHELX. *Acta Crystallogr., Sect. A: Found. Crystallogr.* **2008**, *64* (1), 112−122.

(89) Dolomanov, O. V.; Bourhis, L. J.; Gildea, R. J.; Howard, J. a. K.; Puschmann, H. OLEX2: A Complete Structure Solution, Refinement and Analysis Program. *J. Appl. Crystallogr.* **2009**, *42* (2), 339−341.

(90) Sheldrick, G. M. Crystal Structure Refinement with SHELXL. *Acta Crystallogr., Sect. C: Struct. Chem.* **2015**, *71* (1), 3−8.

(91) Tao, J.; Perdew, J. P.; Staroverov, V. N.; Scuseria, G. E. Climbing the Density Functional Ladder: Nonempirical Meta–Generalized Gradient Approximation Designed for Molecules and Solids. *Phys. Rev. Lett.* **2003**, *91* (14), No. 146401.

(92) Grimme, S.; Ehrlich, S.; Goerigk, L. Effect of the Damping Function in Dispersion Corrected Density Functional Theory. *J. Comput. Chem.* **2011**, *32* (7), 1456−1465.

(93) Neese, F. Software Update: The ORCA Program System—Version 5.0. *WIREs Comput. Mol. Sci.* **2022**, *12* (5), No. e1606.

(94) Weigend, F.; Ahlrichs, R. Balanced Basis Sets of Split Valence, Triple Zeta Valence and Quadruple Zeta Valence Quality for H to Rn: Design and Assessment of Accuracy. *Phys. Chem. Chem. Phys.* **2005**, *7* (18), 3297−3305.

(95) Weigend, F. Accurate Coulomb-Fitting Basis Sets for H to Rn. *Phys. Chem. Chem. Phys.* **2006**, *8* (9), 1057−1065.

(96) Grimme, S. Supramolecular Binding Thermodynamics by Dispersion-Corrected Density Functional Theory. *Chem. - Eur. J.* **2012**, *18* (32), 9955−9964.